HPV-negative, but not HPV-positive, oropharyngeal carcinomas strongly induce fibroblasts to support tumour invasion through micro-environmental release of HGF and IL-6

Robert Bolt[1,*], Bernadette Foran[2], Craig Murdoch[1], Daniel W. Lambert[1], Sally Thomas[3], and Keith D. Hunter[1]

[1] School of Clinical Dentistry, University of Sheffield, Sheffield, South Yorkshire, S10 2TA, UK
[2] Department of Oncology, Western Park Hospital, Sheffield, South Yorkshire, S10 2TA, UK
[3] Department of Biomedical Sciences, University of Sheffield, Sheffield, South Yorkshire, S10 2TN, UK

* To whom correspondence should be addressed. Tel: +44 114 2265463; Fax: +44 114 2717863; Email: r.bolt@sheffield.ac.uk

Short title:

HGF and IL-6 in oropharyngeal carcinoma

Abstract

Human papillomavirus (HPV) infection is causally related to a subset of oropharyngeal carcinomas (OPC) and is linked to a more favourable prognosis compared to HPV-negative OPC. The mechanisms underlying this effect on prognosis are not fully understood but interactions with the tumour microenvironment may be pivotal. Here, we investigated the role of the tumour microenvironment in HPV-positive compared to HPV-negative cancer using 2D and 3D modelling of OPC interactions with stromal fibroblasts. HPV-negative, but not HPV-positive, OPC-derived cell lines induced a rapid fibroblast secretory response that supported 2D cancer cell migration and invasion *in vitro*. Array profiling of this HPV-negative induced fibroblast secretome identified hepatocyte growth factor (HGF) as the principal secreted factor that promoted cancer cell migration. The interaction between HPV-negative cell lines and fibroblasts in 2D was prevented using c-Met (HGF receptor) inhibitors, which further restricted both HPV-negative and positive cell invasion in 3D co-culture models. Furthermore, we discovered a synergistic relationship between HGF and IL-6 in the support of migration that relates JAK activation to HGF responsiveness in HPV-negative lines. In summary, our data show significant differences in the interactions between HPV-positive and HPV-negative OPC cells and stromal fibroblasts. In addition, we, provide *in vitro* evidence to support the clinical application of c-MET inhibitors in the control of early HPV-negative OPC.

Summary

HPV-negative OPC cell lines are capable of rapidly inducing stromal fibroblasts to support tumour migration and invasion, whereas HPV-positive lines have a reduced potential for interaction. HGF is a key factor underling these interactions, and may be supported through IL-6 and JAK signalling.

Introduction

Oropharyngeal carcinoma (OPC) has become a major public health concern as a result of the recent surge of disease linked to Human Papillomavirus (HPV)(1,2). Indeed, OPC now represents the most common malignancy encountered by the head and neck oncologist(3). Much effort has been invested into tailoring therapeutic strategies towards the emerging HPV-positive subset of tumours due to their favourable prognosis and occurrence in younger individuals, whom may therefore suffer greater long-term sequelae of aggressive therapy. Whilst there is an urgent need to optimise management strategies in HPV-positive disease, the poor prognosis of HPV-negative OPC should not be overlooked. Moreover, a recent UK-based study suggests that as well as the well-publicised increase in HPV-positive disease, incidence of HPV-negative oropharyngeal carcinoma is also increasing(4). Comparison of the biology of HPV-positive and -negative disease may offer insights into prognostic determinants, and therefore how best to deliver targeted therapeutics to manage HPV-negative disease.

Although preservation of wild-type TP53, reduced genetic aberration and tumour radiosensitivity account for a significant proportion of the prognostic variation between HPV-positive and -negative disease, much remains unknown about the overall pathogenesis of these malignancies(5-7). Little data is available on the role of the tumour microenvironment in OPC and how this may relate to a HPV-positive tumour status. Recent work has illustrated the significant role of the microenvironment in supporting the progression of poorly prognosticating head and neck cancer, and how this relates to loss of p16 and p53(8). HPV-positive tumours characteristically display upregulated p16 expression and carry wild-type TP53 as a consequence of viral oncogenes E6 and E7 functionally sequestrating important tumour suppressors – thereby abrogating the evolutionary pressure for genetic aberration during tumorigenesis. HPV-positive disease may therefore derive prognostic benefit from a lack of microenvironment interactions attributable to tumour p16 and p53 status, or as a result of viral evasion of the immune system through suppression of inflammatory signalling(9-11). Indeed, HPV is regarded as a strictly epitheliotropic virus(12), and evasion of connective tissue exposure to the virus appears necessary in order to avoid clearance.

The purpose of this study was to investigate the effects of the secretome of both HPV-positive and HPV-negative OPC cell lines on oral and tonsillar fibroblasts harvested from normal tissue. We demonstrate that HPV-negative tumour lines have the ability to induce fibroblasts to develop a secretory phenotype supportive of tumour migration and invasion. Specifically, we show that HPV-negative cell line migration is promoted by inducing fibroblast secretion of a combination of HGF and

IL-6, and that 3D invasion can be restrained by the clinically available c-MET inhibitor, foretinib.

Materials and methods

Cell lines and culture conditions

OPC cell lines UD SCC02, UPCI SCC072, UPCI SCC089 and UPCI SCC090 were received under Material Transfer Agreement from Prof. S. Gollin, University of Pittsburgh School of Public Health, Pittsburgh. HPV status was confirmed by PCR using a commercially-available HPV16 E1 probe (Applied Biosystems, UK) in addition to a custom HPV16 E6 probe using a previously published sequence of 5′-(FAM)- CCCAGAAAGTTACCACAGTTATGCACAGAGCT-(TAMRA)-3′(13). Short tandem repeat (STR) profiling was undertaken to confirm cell line authenticity. A summary of cell lines used in experiments is given in supplementary Table i (14-19).

Fibroblast cultures were derived from oral (DENOF08) and tonsillar (NTF01, NTF06) explant cultures as described previously(20), using surplus tissue retrieved from patients with written, informed consent during routine oral and ENT surgery with ethical approval (09/H1308/66). Both fibroblasts and OPC cell lines were cultured in Dulbecco's Modified Eagle's Medium (DMEM) supplemented with 10 % FCS, with 2 mM L-glutamine & 50 IU penicillin and 50 μg ml^{-1} streptomycin ("normal media") and incubated under standard conditions (5 % CO_2, 37 ℃). All cell cultures were subject to regular mycoplasma testing.

Collection of conditioned medium

Cell lines were grown to approximately 70-90 % confluence in 75 cm^2 flasks, washed three times in PBS and then incubated with fresh normal media for 24 hours. Conditioned medium was then retrieved, centrifuged at 3000 rpm for 5 minutes to remove cell debris and stored at -20 ^oC. Each respective 75 cm^2 flask was trypsinised, cells counted and conditioned medium normalised to a concentration of 3×10^6 cells ml^{-1}.

Collection of stimulated fibroblast medium

Passage 7 oral and tonsillar fibroblast cultures were grown to early confluence in 75 cm^2 flasks, washed X3 in PBS and then incubated with either OPC cell line conditioned media or normal media control for 24 hours. Flasks were then washed X3 in PBS and incubated with normal media for a further 24 hours in order to collect a “stimulated” fibroblast conditioned media. Conditioned media was then retrieved, centrifuged at 3000 rpm for 5 minutes and then stored at -20 ^oC. Each respective 75 cm^2 flask was trypsinised and cells counted in order to confirm an equal number of cells in each experiment post-stimulation. The process of OPC cell line/fibroblast conditioned media collection is summarised in supplemental Figure A.

Re-exposure of cell lines to stimulated fibroblast medium

Each cell line was exposed to either unstimulated fibroblast conditioned medium control or media derived from fibroblasts stimulated by the respective cell line conditioned medium in the subsequent experiments (MTS assay and ORIS^{TM} assay).

MTS assay

Proliferation of UD SCC2, UPCI SCC72, UPCI SCC89 and UPCI SCC90 in the presence of either respective stimulated fibroblast media or unstimulated fibroblast conditioned media control was assessed by means of MTS proliferation assay. Cells were grown to 70-80 % confluence in 75 cm^2 flasks, trypsinised, counted using a haemocytometer, divided, centrifuged at 1000 rpm for 5 minutes, resuspended in the respective stimulated fibroblast or control media, re-counted and then 100 µl of cell suspension seeded at a density of 1 x 10^4 cells per well into a 96-well plate, using triplicate repeats for each condition. Wells were incubated at 37 ^oC in a 5 % CO_2 environment, and time points taken at baseline, 24, 48, 72 and 96 hours in order to assess proliferation over the observed period. At each time point, respective triplicate wells were rinsed with 100 µl PBS, then 100 µl normal media added. MTS (20 µl, CellTiter, Promega, Madison, USA) was then added to each well, and incubated for 1.5 hours. Optical density at 492nm was then measured using a Tecan Infinite M200 plate reader.

2D Cell exclusion zone migration assay

ORIS^{TM} (AMS Biotechnology, Oxford, UK) assay plates were prepared under sterile conditions according to the manufacturer's instructions. 100 µl of each cell line

suspension at a pre-optimised concentration for well confluency was pipetted into respective ORIS™ assay wells and left overnight to adhere. Following cell adherence and confirmation of well confluency, optimised concentrations of mitomycin C in normal media were prepared from snap-frozen stock aliquots stored at -80 °C. Optimisation of mitomycin C-induced growth arrest was undertaken for each cell line using flow cytometric analysis of CellTrace™ (Invitrogen, Life Technologies, Paisley, UK – data not shown). Silicone stoppers were removed from assay wells and normal media carefully aspirated, 2 X 100 µl PBS washes undertaken, and then 100 µl mitomycin C carefully pipetted into respective wells and incubated for 3.5 hours at 37 °C in the dark. Following incubation in mitomycin C, baseline void photomicrographs were taken using a X4 objective lens, assay wells washed X2 in PBS and then 100 µl either stimulated fibroblast conditioned media or unstimulated fibroblast conditioned media control pipetted into respective wells. ORIS™ assay plates were incubated for either 20 hours (UPCI SCC089 – a rapidly migrating line under basal conditions) or 48 hours (UD SCC02, UPCI SCC072, UPCI SCC090) in order for migration to occur, and then endpoint photomicrographs taken using a X4 objective lens. Area of exclusion zone closure over the experimental period was measured using ImageJ (freeware, NIH, USA).

Experiments were repeated for recombinant protein dose-response analysis using recombinant human CTGF, CXCL1, CXCL2, CXCL3, CXCL5, CXCL6, HGF, IL-6, IL-8, OPG and OSM (Insight Biotechnology, Wembley, UK) in place of stimulated fibroblast media. Inhibitor analysis was also undertaken as outlined above with the addition of either DMSO control or foretinib (0.4, 4 or 40 nM)/ruxolitinib (1 µM) to conditioned media over the period of migration.

Cytokine array

Serum-free conditioned media were collected from cell lines and stimulated fibroblasts in the same manner as described above and analysed by cytokine array (C6-8 array, Ray biotechnology) following the manufacturer's protocol.

Flow cytometry

Cell lines UD SCC2, UPCI SCC072, UPCI SCC089 and UPCI SCC090 were grown to 70-80 % confluence in 75 cm^2 flasks, along with HeLa and HepG2 controls. Cells were removed from respective flasks using EDTA cell dissociation solution (Sigma-Aldrich, Dorset, UK), suspended in FACS buffer (PBS with 0.1 % Sodium Azide, 1 % BSA) cooled on ice, and centrifuged at 1000 rpm for 5 minutes. The supernatant was then decanted and cells resuspended in 900 µl cooled FACS buffer. Each cell suspension was then divided equally into three microtubes and centrifuged at 2000 rpm for 2 minutes. Following careful aspiration of supernatant, cells were resuspended in 100 µl cooled FACS buffer containing either no additive, 1.0 µg ml^{-1} FITC-conjugated c-Met probe, or 1.0 µg ml^{-1} rat IgG1κ isotype control (e-Bioscience, Hatfield, UK). Each suspension was then incubated on ice and in the dark for 40 minutes. Following incubation, cells were centrifuged at 2000 rpm for 2 minutes, supernatants carefully aspirated and cell pellets resuspended in 1000 µl cold FACS buffer. A repeat centrifugation and cold FACS buffer wash was undertaken, followed by final centrifugation at 2000 rpm for 2 minutes, aspiration of supernatant and then resuspension in 300 µl cold FACS buffer. Cells were then analysed using a Calibur

flow cytometer (Becton Dickinson). Flow cytometry data were interpreted using Flowing 2.5.1 software (Freeware, Turku, Finland).

Western blotting

Cell lines were grown in 75cm flasks to approximately 70% confluence. Cultures were washed in PBS and then exposed to either unstimulated fibroblast conditioned medium control or stimulated fibroblast conditioned medium for 0 mins, 20 mins or 12 hrs. On completion of each respective incubation period, flasks were washed in cold TBS and then incubated with 1ml cell dissociation solution at 4 ^{o}C on a rocking machine for 10 mins. Cells were then added to a microtube and centrifuged at 1,000 rpm for 5 mins. Cell pellets were lysed on ice in a buffer containing 50mM Tris HCL pH 7.4, 250mM NaCl, 5mM EDTA, 0.3% Triton X-100 and EDTA-free protease inhibitor cocktail (Roche, Germany).

Samples were then boiled for 5 minutes in an equal volume of Laemmli sample buffer, and separated using pre-cast gels (Mini-Protean TGX, Bio-Rad, California, USA). Separated samples were transferred to a nitrocellulose membrane (Amersham Hybond ECL, GE Healthcare, Chicago, USA), membranes blocked for thirty minutes in 5% skimmed milk in Tris buffered saline (pH 7.4) with 0.1% Tween-20, then incubated with either Tyr 705-phosphorylated/non-phospho specific STAT3 antibodies (Cell Signalling Technology, Danvers, USA; both antibodies used at 1: 1000 dilution) or anti-β actin control (1:2000 dilution) in 5% BSA/TBST overnight at 4 ^{o}C. Membranes were then incubated with horseradish peroxidase conjugated

secondary antibody at a dilution of 1:10 000 for 45 mins and imaged using ECL reagent (GE Healthcare).

3D invasion assay

Culturex^{TM} 3D invasion assays (AMS Biotechnology, Oxford, UK) were prepared following manufacturer's instructions. Passage 7 DENOF08 normal oral fibroblasts and cell lines were grown to approximately 70 % confluence in separate 75 cm^2 flasks. Each cell culture was trypsinised, centrifuged at 1000 rpm for 5 minutes, resuspended in normal media and counted. An appropriate volume of each cell suspension was then pipetted into universal containers along with 4 ml normal media minus the volume of cell suspension pipetted in order to achieve a final cell concentration of 6 x 10^4 cells ml^{-1}. Two further cell suspensions containing both DENOF08 normal oral fibroblasts mixed with each cell line were created in an identical manner. DENOF08 fibroblasts were mixed to each cell line in a ratio of 1:6. Cultrex^{TM} invasion assays were then undertaken according to manufacturer's instructions using HPV-negative cell lines either alone, or in combination with mixed fibroblasts. DMSO control or 60 nM foretinib were added to wells at the start of invasion. Day 6 Inverted lens micrographs were analysed using ImageJ software and number of invading cells counted as described by Rudisch *et al* (21).

Statistical Analyses

Statistical analysis was undertaken using SPSS Version 22, (IBM, Chicago, USA). Probability of <0.05 was considered statistically significant. Analysis of migration was

undertaken using the Mann Whitney *U*-test for non-parametric data. Analysis of proliferation was undertaken using the Student's t-test for parametric data.

Results

1. HPV-negative OPC lines induce a fibroblast phenotype that supports tumour migration, whereas HPV-positive OPC lines do not

Fibroblast cultures stimulated by HPV-negative OPC cell lines produced conditioned media that was supportive of cancer cell migration when re-exposed to the respective stimulating carcinoma cell line. HPV-positive OPC cell lines did not stimulate a significant fibroblast response and did not induce migration (Figure 1A). Support of migration was consistently observed using a range of stimulated oral (DENOF08) and tonsil fibroblast cultures (NTF01, NTF06) (Figure 1A). Although a weak trend towards increased proliferation was noted with all stimulated fibroblast media, with cell lines UPCI SCC090 and UPCI SCC072 demonstrating significant increases ($P<0.05$) in proliferation at 96 hours, MTS assay demonstrated no significant difference in proliferative response of HPV-negative cell lines in comparison to HPV-positive cell lines (Figure 1B-E).

2. HPV-negative OPC cell lines stimulate normal oral fibroblasts to adopt a characteristic secretory profile when compared to HPV-positive OPC lines

Cytokine array analysis of stimulated fibroblast conditioned medium was undertaken to investigate changes in the fibroblast secretome that may account for differences in

cancer cell migration. Conditioned media taken from fibroblasts stimulated by HPV-negative cell lines demonstrated a characteristic secretory profile compared to HPV-positive lines (Figure 2 A-D). Densitometry of cytokine array data identified upregulation of a number of factors that signal via CXCR-1/2, including IL-8, CXCL6, CXCL5, CXCL1 and GRO (CXCL1-3; array spot non-specific to GRO subtype). HGF and IL-6 were also secreted in greater amounts by fibroblasts in response to HPV-negative compared to HPV-positive cell line stimulation, with a similar secretory profile being observed in both oral and tonsillar fibroblasts. To examine which factor(s) in stimulated fibroblast conditioned media were responsible for driving migration, dose-response analysis was undertaken on cell line UPCI SCC072 using recombinant candidate proteins identified as upregulated in the cytokine arrays. Dose-response analysis established two factors capable of driving cell line migration, namely HGF and Oncostatin M (OSM) (Figure 3 A). Subsequent ELISA analysis found OSM to be absent from stimulated fibroblast conditioned media (data not shown).

3. HPV-negative OPC lines induce fibroblasts to release HGF. Inhibition of HGF leads to abrogation of fibroblast support of HPV-negative cell line migration and invasion

ELISA analysis demonstrated minimal release of HGF in both OPC cell lines and fibroblasts when cultured alone (Figure 3B). However, stimulation of fibroblasts with cell line conditioned media led to a significant increase in HGF production, with marked HGF release by fibroblasts in response to media taken from HPV-negative cell lines when compared to fibroblasts stimulated by media from HPV-positive cell

lines (Figure 3 B). HGF secretion occurred within the first 24 hours of fibroblast stimulation, and was noted to be elevated in cell line conditioned media following subsequent co-incubation with fibroblasts (Figure 3 B, “mixed media”). Although an HGF response was observed in fibroblasts following stimulation by HPV-positive cell lines, the response was much reduced within the 24 hour period post-stimulation (Figure 3 B). Expression levels of the HGF receptor, c-Met, were comparable in all OPC lines (Figure 3C).

c-Met activation leads to the phosphorylation of a number of intracellular signalling molecules, including STAT3. To examine secondary messenger activation of cell lines in response to stimulated fibroblast conditioned media, immunoblotting for phosphorylated (p)STAT3 was performed (Figure 3D), demonstrating marked elevation of pSTAT3 in HPV-negative cell lines following 20 minutes’ exposure to stimulated fibroblast media. Although elevated compared to baseline, HPV-positive cell lines did not display the same degree of STAT3 phosphorylation at 20 minutes. A single cell line, UPCI SCC089, demonstrated basal pSTAT3 expression.

Exposure of HPV-negative cell lines to progressive doses of the c-MET inhibitor foretinib led to near total abrogation of cell migration in response to stimulated fibroblast conditioned media at 40 nM (Figure 4 A&B). Analysis of LDH activity in the conditioned media indicated the inhibitors were not cytotoxic at the doses used (supplemental data). As foretinib has minor potency on EGFr, cell migration experiments were repeated in normal media containing 20 ng ml^{-1} recombinant EGF. Incubation with 20 ng ml-1 EGF demonstrated an increase in overall migration, which was not reduced following exposure to foretinib in concentrations equal to that used to abrogate migration in stimulated fibroblast media, confirming that EGF was

not responsible for fibroblast-induced migrations. EGF ELISA analysis further confirmed the absence of EGF from stimulated fibroblast media. Experiments were further repeated with the highly-specific c-MET inhibitor, INCB28060 (Capmatinib), with an identical pattern of effect to that observed with foretinib (data not shown).

Invasion was observed in spheroid models when HPV-negative cell lines were co-cultured with normal fibroblasts, whereas minimal invasion was noted in cell lines in the absence of fibroblasts (Figure 5 A&C). Cells invading into the collagen matrix demonstrated cytokeratin A1/3 positivity upon immunohistochemical analysis, confirming cell lines had invaded (supplemental Figure D). Exposure to 60 nM foretinib significantly ($p<0.001$) reduced invasion of co-cultured HPV-negative cell lines (Figure 5 D). Compared to HPV-negative cell lines, HPV-positive cell lines demonstrated significantly ($p<0.05$) less invasion. Overall, the amount of invasion observed in all cell lines was consistent with the amount of HGF induced in fibroblast conditioned media as measured via ELISA in 2D experiments (Figure 3 B).

4. IL-6/JAK activation leads to support of HGF-induced migration in HPV-negative cell lines

Due to discrepancies between ELISA-measured HGF concentration in stimulated fibroblast media linked to cell line UPCI SCC072 and the concentration of recombinant HGF required to induce the same degree of migration in the aforementioned cell line, IL-6 was investigated as a candidate molecule for supplementing HGF's effect. IL-6 was observed to be elevated in HPV-negative stimulated fibroblast media in a similar manner to HGF although addition of

recombinant IL-6 alone failed to induce migration (Figure 3A). Addition of recombinant IL-6 to HGF potentiated HGF's effect on migration in cell line UPCI SCC072 (Figure 6 A). Ruxolitinib, a JAK inhibitor capable of blocking IL-6 induced STAT3 activation whilst permitting continued HGF activation of STAT3 via a JAK-independent route, confirmed that inhibition of JAK activity reduced cell line responsiveness to stimulated fibroblast media (Figure 4 C&D).

In the case of HPV-negative cell line UPCI SCC089 (observed to be unresponsive to recombinant IL-6 supplementation of HGF), inhibition of basal JAK activity was considered the mechanism through which ruxolitinib had achieved an inhibitory effect – indeed, this finding is consistent with Western blot data which demonstrate basal STAT3 activation in this cell line (Figure 3 D).

Discussion

Our data demonstrate for the first time that HPV-negative tumour lines have greater capacity compared with HPV-positive lines to rapidly induce a normal fibroblast population to produce a pro-invasive secretome. Whilst stromal support of tumour invasion has been classically ascribed to established cancer-associated fibroblasts(22), it appears that a phenotypically mature cancer-associated stromal population is unnecessary. Although it is likely that cancer-associated fibroblasts represent a more established secretory phenotype, and may be both autonomous and more exaggerated in their factor secretion compared to the stimulated normal stroma, it is possible that senescent and myo-fibroblastic cancer-associated

fibroblast populations(23) are the downstream consequence of pathways utilised to immediately recruit normal stroma into supporting tumour progression. Indeed, the capacity of a rapid fibroblast HGF-secreting response offers clear selection pressure for tumour populations to evolve towards stromal activation, whereas the more gradual process of cancer-associated fibroblast formation offers a less immediate evolutionary advantage.

A recent review has highlighted the importance of c-MET signalling in both malignant and stromal cells of the head and neck region(24). Our work suggests that HGF upregulation is a characteristic feature of HPV-negative, but not HPV-positive OPC and may contribute to its more aggressive nature compared to HPV-positive disease. Indeed, Kwon *et al.* published clinical data suggesting immunohistochemical HGF status but not c-Met status is predictive of HPV-negative tumour outcomes, although neither HGF nor c-Met are predictive in HPV-positive disease(25). This is consistent with our findings, which demonstrated comparable c-Met status in all OPC lines analysed, in addition to fibroblast secretion of HGF supporting HPV-negative cell line migration. Whilst HPV-positive cell lines also appear to be capable of inducing a HGF response in fibroblasts, the magnitude of response *in vitro* is low compared to that of HPV-negative cells and may account for the lack of predictive value related to a positive HGF status in HPV-positive disease. HPV-positive disease is well-documented as presenting at a more advanced nodal stage than HPV-negative disease – whilst this observation appears counterintuitive to our *in vitro* findings, it should be noted that our model of HGF induction relates to additional rather than overall migration; no relationship was noted in stimulated/unstimulated migration rates when compared between cell lines. In the case of HPV-positive disease,

migratory and invasive potential may be independent of HGF, although may still remain clinically more extensive than observed in HPV-negative disease.

Our 3D invasion experiments suggest foretinib offers much promise in the management of HPV-negative OPC. Relatively modest results have been observed with foretinib in clinical trials although all current Phase II studies have investigated advanced and metastatic disease(26-29). A more appropriate strategy for the application of c-MET inhibitors may be in the management of early stage tumours, whereby obstructing migration and invasion of OPC cells may lead to reduced metastasis and more manageable local disease. Interestingly, foretinib restricted 3D co-culture invasion in similar concentrations to that observed in 2D models. This finding may be due to the fact that the functional effect of foretinib has been measured through analysis of cellular escape from a tumour spheroid surface, whereby a number of the features of 3D tumour drug resistance which often protect cells at the central core of spheroids, such as concentration gradients and hypoxic barriers, are no longer relevant. c-MET inhibitors may therefore serve as an ideal candidate for the limit of tumour spread *in vivo*.

We present data to support a complex interrelationship between HGF and HPV-negative OPC motility; basal JAK activity and IL-6 both appear to have a significant role in supporting cell responsiveness to HGF, and may offer potentiation of HGF signalling through common secondary messenger systems such as STAT3. Crosstalk between HGF and other signalling systems has been recognised as a major mechanism in the progression of human cancer(30); indeed, Hov *et al.* noted cooperation between HGF and IL-6 in supporting migration of the myeloma line INA-6 in a similar manner to that observed with cell line UPCI SC072(31), although these

investigators proposed the supporting effects of IL-6 were attributable to induction of c-Met expression rather than direct interplay of secondary messenger systems. Our finding that JAK inhibition reduces HGF responsiveness in HPV-negative cell lines suggests that JAK-dependent secondary messenger systems are necessary for this supplemental effect, although we have not excluded induction of c-Met expression as the downstream mechanism through which this interaction is achieved. Ruxolitinib's effect on HPV-negative cell line migration in response to stimulated fibroblast media is consistent with the subtle differences between HGF and IL-6 induction of STAT3, and may infer a STAT3 basis of HGF/IL-6 cooperativity. This model requires further validation in the context of a number of other signalling molecules phosphorylated by JAKs.

Our data suggest that c-Met inhibitors such as foretinib may be of particular clinical value as an adjuvant to current protocols in the management of early HPV-negative OPC. Restraint of early tumour invasion through HGF inhibition may create more manageable local disease in addition to reducing micro-metastasis. Further, *in-vivo* pre-clinical data is necessary to determine whether c-Met inhibitors have the same capacity to restrict OPC invasion using an animal model, as has been observed *in-vitro*.

Funding

Robert Bolt was supported by a Joint Cancer Research UK and Yorkshire Cancer Research Clinical Doctoral Training Fellowship Grant (R/132590-11-12).

Acknowledgements

The authors would like to thank Dr Jill Callaghan and Dr Vanessa Hearnden for their assistance with tissue culture experiments.

Conflict of Interest Statement: None declared.

References

1. Marur, S*., et al.* (2010) HPV-associated head and neck cancer: a virus-related cancer epidemic. *Lancet Oncol*, **11**, 781-9.
2. Näsman, A*., et al.* (2009) Incidence of human papillomavirus (HPV) positive tonsillar carcinoma in Stockholm, Sweden: an epidemic of viral-induced carcinoma? *Int J Cancer*, **125**, 362-6.
3. Kumar, B*., et al.* (2015) Surgical management of oropharyngeal squamous cell carcinoma: Survival and functional outcomes. *Head Neck*.
4. Schache, A.G*., et al.* (2016) HPV-Related Oropharynx Cancer in the United Kingdom: An Evolution in the Understanding of Disease Etiology. *Cancer Res*, **76**, 6598-6606.
5. Lindel, K*., et al.* (2001) Human papillomavirus positive squamous cell carcinoma of the oropharynx: a radiosensitive subgroup of head and neck carcinoma. *Cancer*, **92**, 805-13.
6. Mirghani, H*., et al.* (2015) Increased radiosensitivity of HPV-positive head and neck cancers: Molecular basis and therapeutic perspectives. *Cancer Treat Rev*, **41**, 844-52.
7. Braakhuis, B.J*., et al.* (2004) Genetic patterns in head and neck cancers that contain or lack transcriptionally active human papillomavirus. *J Natl Cancer Inst*, **96**, 998-1006.
8. Hassona, Y*., et al.* (2013) Progression of genotype-specific oral cancer leads to senescence of cancer-associated fibroblasts and is mediated by oxidative stress and TGF-β. *Carcinogenesis*, **34**, 1286-95.
9. Richards, K.H*., et al.* (2014) Human papillomavirus E7 oncoprotein increases production of the anti-inflammatory interleukin-18 binding protein in keratinocytes. *J Virol*, **88**, 4173-9.
10. Tummers, B*., et al.* (2015) High-risk human papillomavirus targets crossroads in immune signaling. *Viruses*, **7**, 2485-506.
11. Gosmann, C*., et al.* (2014) IL-17 suppresses immune effector functions in human papillomavirus-associated epithelial hyperplasia. *J Immunol*, **193**, 2248-57.
12. zur Hausen, H. (2000) Papillomaviruses causing cancer: evasion from host-cell control in early events in carcinogenesis. *J Natl Cancer Inst*, **92**, 690-8.

13. Zhao, M.*, et al.* (2005) Feasibility of quantitative PCR-based saliva rinse screening of HPV for head and neck cancer. *Int J Cancer*, **117**, 605-10.
14. Ragin, C.C.*, et al.* (2004) Mapping and analysis of HPV16 integration sites in a head and neck cancer cell line. *Int J Cancer*, **110**, 701-9.
15. Ferris, R.L.*, et al.* (2005) Human papillomavirus-16 associated squamous cell carcinoma of the head and neck (SCCHN): a natural disease model provides insights into viral carcinogenesis. *Eur J Cancer*, **41**, 807-15.
16. White, J.S.*, et al.* (2007) The influence of clinical and demographic risk factors on the establishment of head and neck squamous cell carcinoma cell lines. *Oral Oncol*, **43**, 701-12.
17. Lin, C.J.*, et al.* (2007) Head and neck squamous cell carcinoma cell lines: established models and rationale for selection. *Head Neck*, **29**, 163-88.
18. Virgilio, L.*, et al.* (1996) FHIT gene alterations in head and neck squamous cell carcinomas. *Proc Natl Acad Sci U S A*, **93**, 9770-5.
19. Wald, A.I.*, et al.* (2011) Alteration of microRNA profiles in squamous cell carcinoma of the head and neck cell lines by human papillomavirus. *Head Neck*, **33**, 504-12.
20. Colley, H.E.*, et al.* (2011) Development of tissue-engineered models of oral dysplasia and early invasive oral squamous cell carcinoma. *Br J Cancer*, **105**, 1582-92.
21. Rudisch, A.*, et al.* (2015) High EMT Signature Score of Invasive Non-Small Cell Lung Cancer (NSCLC) Cells Correlates with NFκB Driven Colony-Stimulating Factor 2 (CSF2/GM-CSF) Secretion by Neighboring Stromal Fibroblasts. *PLoS One*, **10**, e0124283.
22. De Wever, O.*, et al.* (2008) Stromal myofibroblasts are drivers of invasive cancer growth. *Int J Cancer*, **123**, 2229-38.
23. Mellone, M.*, et al.* (2016) Induction of fibroblast senescence generates a non-fibrogenic myofibroblast phenotype that differentially impacts on cancer prognosis. *Aging (Albany NY)*, **9**, 114-132.
24. Szturz, P.*, et al.* (2017) Understanding c-MET signalling in squamous cell carcinoma of the head & neck. *Crit Rev Oncol Hematol*, **111**, 39-51.
25. Kwon, M.J.*, et al.* (2014) Frequent hepatocyte growth factor overexpression and low frequency of c-Met gene amplification in human papillomavirus-negative tonsillar squamous cell carcinoma and their prognostic significances. *Hum Pathol*, **45**, 1327-38.
26. Choueiri, T.K.*, et al.* (2013) Phase II and biomarker study of the dual MET/VEGFR2 inhibitor foretinib in patients with papillary renal cell carcinoma. *J Clin Oncol*, **31**, 181-6.
27. Shah, M.A.*, et al.* (2013) Phase II study evaluating 2 dosing schedules of oral foretinib (GSK1363089), cMET/VEGFR2 inhibitor, in patients with metastatic gastric cancer. *PLoS One*, **8**, e54014.
28. Seiwert, T.*, et al.* (2013) Phase II trial of single-agent foretinib (GSK1363089) in patients with recurrent or metastatic squamous cell carcinoma of the head and neck. *Invest New Drugs*, **31**, 417-24.
29. Rayson, D.*, et al.* (2016) Canadian Cancer Trials Group IND197: a phase II study of foretinib in patients with estrogen receptor, progesterone receptor, and human epidermal growth factor receptor 2-negative recurrent or metastatic breast cancer. *Breast Cancer Res Treat*, **157**, 109-16.
30. Gherardi, E.*, et al.* (2012) Targeting MET in cancer: rationale and progress. *Nat Rev Cancer*, **12**, 89-103.
31. Hov, H.*, et al.* (2009) c-Met signaling promotes IL-6-induced myeloma cell proliferation. *Eur J Haematol*, **82**, 277-87.

TABLE AND FIGURE LEGENDS

Fig. 1. Influence of respective stimulated fibroblast conditioned media on cell lines. (**A**) Additional percentage ORIS^{TM} migration assay void closure compared to unstimulated fibroblast conditioned media control. Prefix denotes cell line – UD/UPCI SCC02, 72, 89 & 90; Suffix denotes fibroblast culture stimulated – DENOF8/NTF 1 & 6. Shaded bars represent HPV-negative cell line data, unshaded bars represent HPV-positive cell line data. n=9, *P ≤ 0.05, **P ≤ 0.01, ***P ≤ 0.001 Mann-Whitney U-test (non-parametric data) (**B-E**) MTS assay of cell lines exposed to stimulated fibroblast media versus unstimulated fibroblast conditioned media control. Circular plots represent stimulated fibroblast media; square plots represent normal media control. n=9, *P ≤ 0.05, **P ≤ 0.01, ***P ≤ 0.001 Students T-test (parametric data).

Fig. 2. Analysis of stimulated fibroblast conditioned media; (**A**) Raybiotech C6 cytokine array; *Ctrl* denotes unstimulated fibroblast conditioned media control, (**B**) C6 array map depicting factors linked to noteworthy uptake in bold (GCP-2 = CXCL-

6)(**C**) Raybiotech C7 cytokine array; *Ctrl* denotes unstimulated fibroblast conditioned media control, (**D**) C7 array map depicting factors linked to noteworthy uptake in bold (ENA-78 = CXCL-5; GRO-α = CXCL-1; GRO = spot responsive to CXCLs-1, 2 &3, (**E**) Raybiotech C6 and C7 cytokine array densitometry (arbitrary units) of those array spots demonstrating differences in response to HPV-positive versus HPV-negative cell line conditioned media.

Fig. 3. Analysis of HGF's role in conditioned media experiments. (**A**) UPCI SCC072 dose-response migration curves for candidate proteins (n=3 biological repeats for each protein at each respective concentration, median value plotted) (**B**) HGF ELISA of cell line conditioned media before – *"cell line media"* and after – *"mixed media"* exposure to fibroblasts, in addition to stimulated fibroblast media – *"fib media".* Note that the initial fibroblast secretory response observed in *"mixed media"* leads to elevated HGF for all cell lines, although HGF release is more pronounced in response to HPV-negative cell lines and furthermore remains sustained into the period 24hrs post-stimulation leading to HGF release into the stimulated fibroblast conditioned media. (**C**) flow cytometric analysis of c-Met status: shaded area represents overlay histogram plot for c-Met probe, unshaded plots represent isotype control probe and control without probe (near-coincidental plots throughout illustrated histograms). Suffices indicate cell lines e.g. *SCC2* = UPCI SCC02. All OPC cell lines expressed c-Met, with no difference in expression noted between HPV-positive and -negative lines. (**D)** & **(E**) total STAT3 and phospho-STAT3 Western blotting of cell lines exposed to respective stimulated fibroblast media: *C* – unstimulated control, *I* – initial response following 20 mins exposure to stimulated fibroblast media, *D* –

delayed response taken following 12h exposure to stimulated fibroblast media. Note the marked initial phospho-STAT3 response in HPV-negative cell lines UPCI SCC089 and UPCI SCC072.

Fig. 4. (**A**) & (**B**) Effect of addition of progressive concentrations of foretinib on cell line migration in response to stimulated fibroblast media in cell lines UPCI SCC072 and UPCI SCC089, respectively. (**C**) & (**D**) Effect of addition of 1μM ruxolitinib on cell line migration in response to stimulated fibroblast media in cell lines UPCI SCC072 and UPCI SCC089, respectively. For all experiments, n=9, Mann-Whitney U-Test utilised as measure of statistical significance, *P ≤ 0.05, **P ≤ 0.01, ***P ≤ 0.001, *CM* denotes stimulated fibroblast conditioned media, *Ctrl* denotes unstimulated control fibroblast conditioned media, *Rux* denotes addition of 1μM ruxolitinib, *For* denotes foretinib with suffix denoting concentration in nM, *DMSO* denotes dimethyl suphoxide solvent control.

Fig. 5. 3D modelling of the effects of foretinib on tumour invasion. (**A-D**) UPCI SCC072 Day 6 Cultrex^{TM} 3D invasion assay, field width=1000 μm: (**A**) Cell line spheroid exposed to DMSO control, (**B**) Cell line spheroid exposed to 60 nM foretinib, (**C**) Cell line/fibroblast co-culture exposed to DMSO control, (**D**) Cell line/fibroblast co-culture exposed to 60nM foretinib. (**E**) Bar chart summarising data for all HPV-positive (unshaded bars) and HPV-negative (shaded bars) cell lines; n=9, * P ≤ 0.05, ***P ≤ 0.001 Mann-Whitney U-test.

Fig.6. Migration of HPV-negative cell lines (**A**) UPCI SCC072 (**B**) UPCI SCC089 in response to incubation with increasing concentrations of recombinant HGF alone (broken line) or in combination with recombinant IL-6.

Supplemental Data:

Table i. Summary of cell lines.

Supplemental Figure A. Process of conditioned media collection

Supplemental Figures B & C. Lactate dehydrogenase (LDH) assays for HPV-negative cell lines exposed to foretinib. (A) LDH assay of cell line UPCI SCC072 exposed to foretinib 0.4-4000 nM. (B) LDH assay of cell line UPCI SCC089 exposed to foretinib 0.4-4000 nM.

Supplemental Figure D. Cytokeratin A1/3 immunohistochemical analysis of tumour spheroid and surrounding invasion matrix; invading cells demonstrate strong cytokeratin A1/3 positivity.

Supplemental Figure E. Phospho c-Met Western Blot of unstimulated cell lines, confirming low basal c-Met phosphorylation in all lines

Fig. 1.

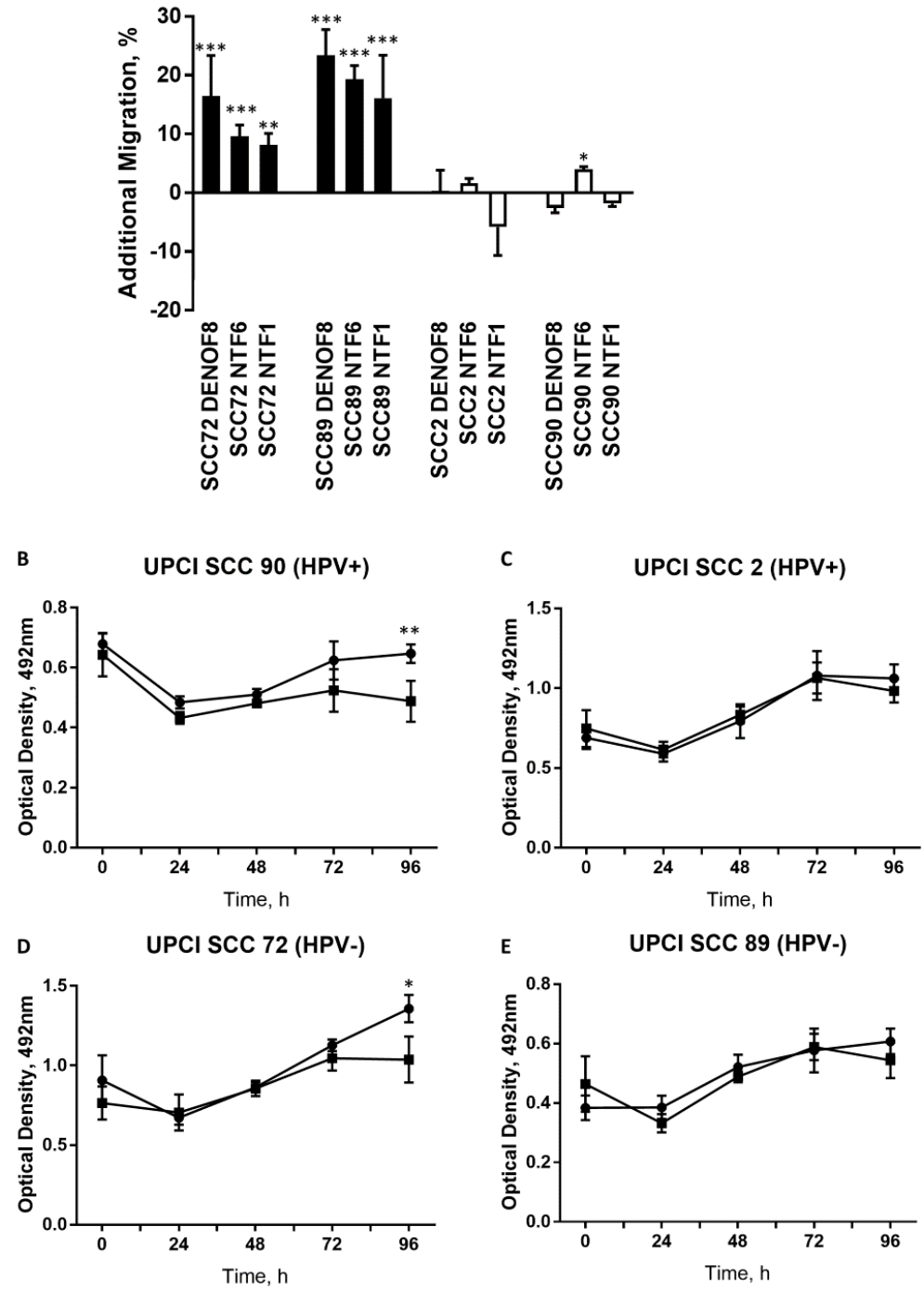
A
Additional Migration, %
30
20
10
0
-10
-20
***
***
**
***
***
***
*
SCC72 DENOF8
SCC72 NTF6
SCC72 NTF1
SCC89 DENOF8
SCC89 NTF6
SCC89 NTF1
SCC2 DENOF8
SCC2 NTF6
SCC2 NTF1
SCC90 DENOF8
SCC90 NTF6
SCC90 NTF1
B
UPCI SCC 90 (HPV+)
Optical Density, 492nm
Time, h
**
C
UPCI SCC 2 (HPV+)
Optical Density, 492nm
Time, h
D
UPCI SCC 72 (HPV-)
Optical Density, 492nm
Time, h
*
E
UPCI SCC 89 (HPV-)
Optical Density, 492nm
Time, h
0
24
48
72
96

Fig 2.

A Ctrl SCC72 HPV- SCC89 HPV- SCC2 HPV+ SCC90 HPV+

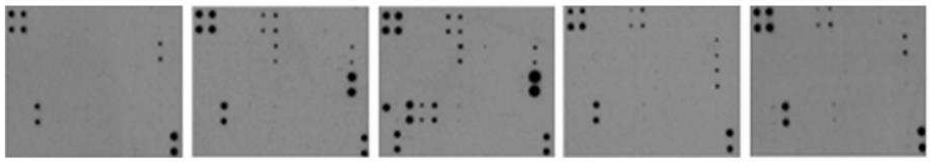

B

	A	B	C	D	E	F	G	H	I	J	K	L	M	N
1	POS	POS	NEG	NEG	BLANK	ANG	BDNF	BLC	BMP4	BMP6	CCL23	CNTF	EGF	Eotaxin 1
2	POS	POS	NEG	NEG	BLANK	ANG	BDNF	BLC	BMP4	BMP6	CCL24	CNTF	EGF	Eotaxin 1
3	Eotaxin 2	Eotaxin 3	FGF-6	FGF-7	Fit-3 Ligand	Fractalkine	GCP-2	GDNF	GM CSF	I-309	IFNγ	IGFBP 1	IGFBP 2	IGFBP 4
4	Eotaxin 2	Eotaxin 3	FGF-6	FGF-7	Fit-3 Ligand	Fractalkine	GCP-2	GDNF	GM CSF	I-309	IFNγ	IGFBP 1	IGFBP 2	IGFBP 4
5	IGF-1	IL-10	IL-13	IL-15	IL-16	IL-1α	IL-1β	IL-1ra	IL-2	IL-3	IL-4	IL-5	IL-6	IL-7
6	IGF-1	IL-10	IL-13	IL-15	IL-16	IL-1α	IL-1β	IL-1ra	IL-2	IL-3	IL-4	IL-5	IL-6	IL-7
7	Leptin	LIGHT	MCP-1	MCP-2	MCP-3	MCP-4	M-CSF	MDC	MIG	MIP-1δ	MIP-3α	NAP-2	NT-3	PARC
8	Leptin	LIGHT	MCP-1	MCP-2	MCP-3	MCP-4	M-CSF	MDC	MIG	MIP-1δ	MIP-3α	NAP-2	NT-3	PARC
9	PDGFBB	RANTES	SCF	SDF-1α	TARC	TGF-β1	TGF-β3	TNF-α	TNF-β	BLANK	BLANK	BLANK	BLANK	POS
10	PDGFBB	RANTES	SCF	SDF-1α	TARC	TGF-β1	TGF-β3	TNF-α	TNF-β	BLANK	BLANK	BLANK	BLANK	POS

C Ctrl SCC72 HPV- SCC89 HPV- SCC2 HPV+ SCC90 HPV+

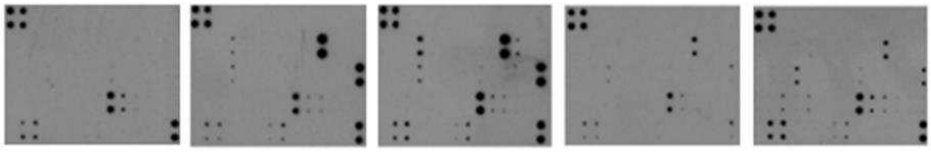

D

	A	B	C	D	E	F	G	H	I	J	K	L	M	N
1	POS	POS	NEG	NEG	BLANK	Arp30	AgRP	ANGPT2	AREG	Axl	bFGF	b-NGF	BTC	CCL28
2	POS	POS	NEG	NEG	BLANK	Arp30	AgRP	ANGPT3	AREG	Axl	bFGF	b-NGF	BTC	CCL28
3	CTAK	Dtk	EGFR	ENA-78	Fas	FGF-4	FGF-9	G-CSF	GITR Ligand	GITR	GRO	GRO-α	HCC-4	HGF
4	CTAK	Dtk	EGFR	ENA-78	Fas	FGF-4	FGF-9	G-CSF	GITR Ligand	GITR	GRO	GRO-α	HCC-4	HGF
5	ICAM-1	ICAM-3	IGFBP-3	IGFBP-6	IGF-1 sR	IL-1 R4	IL-1 R1	IL-11	IL-12 p40	IL-12 p70	IL-17	IL-2Rα	IL-6R	IL-8
6	ICAM-1	ICAM-3	IGFBP-3	IGFBP-6	IGF-1 sR	IL-1 R4	IL-1 R1	IL-11	IL-12 p40	IL-12 p70	IL-18	IL-2Rα	IL-6R	IL-8
7	I-TAC	XCL1	MF	MIP-1α	MIP-1β	MIP-3β	MSPα	NT-4	OPG	OSM	PLGF	sgp130	sTNFRII	sTNFRI
8	I-TAC	XCL1	MF	MIP-1α	MIP-1β	MIP-3β	MSPα	NT-4	OPG	OSM	PLGF	sgp130	sTNFRII	sTNFRI
9	TECK	TIMP-1	TIMP-2	THPO	TRAIL R3	TRAIL R4	uPAR	VEGF	VEGF-D	BLANK	BLANK	BLANK	BLANK	POS
10	TECK	TIMP-1	TIMP-2	THPO	TRAIL R3	TRAIL R4	uPAR	VEGF	VEGF-D	BLANK	BLANK	BLANK	BLANK	POS

E

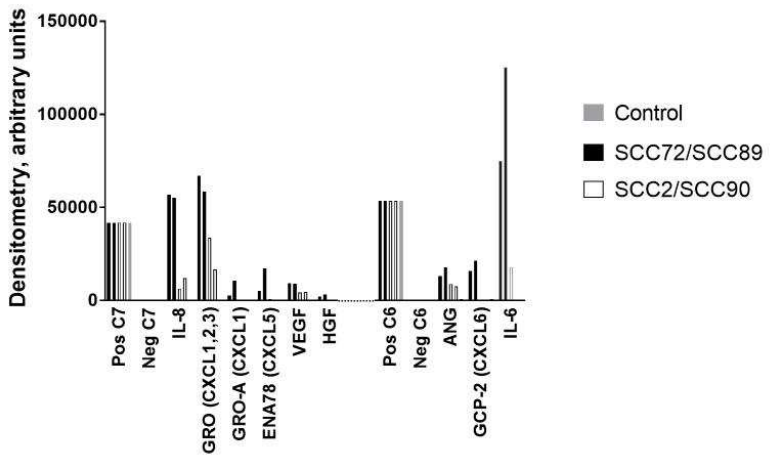

Fig. 3.

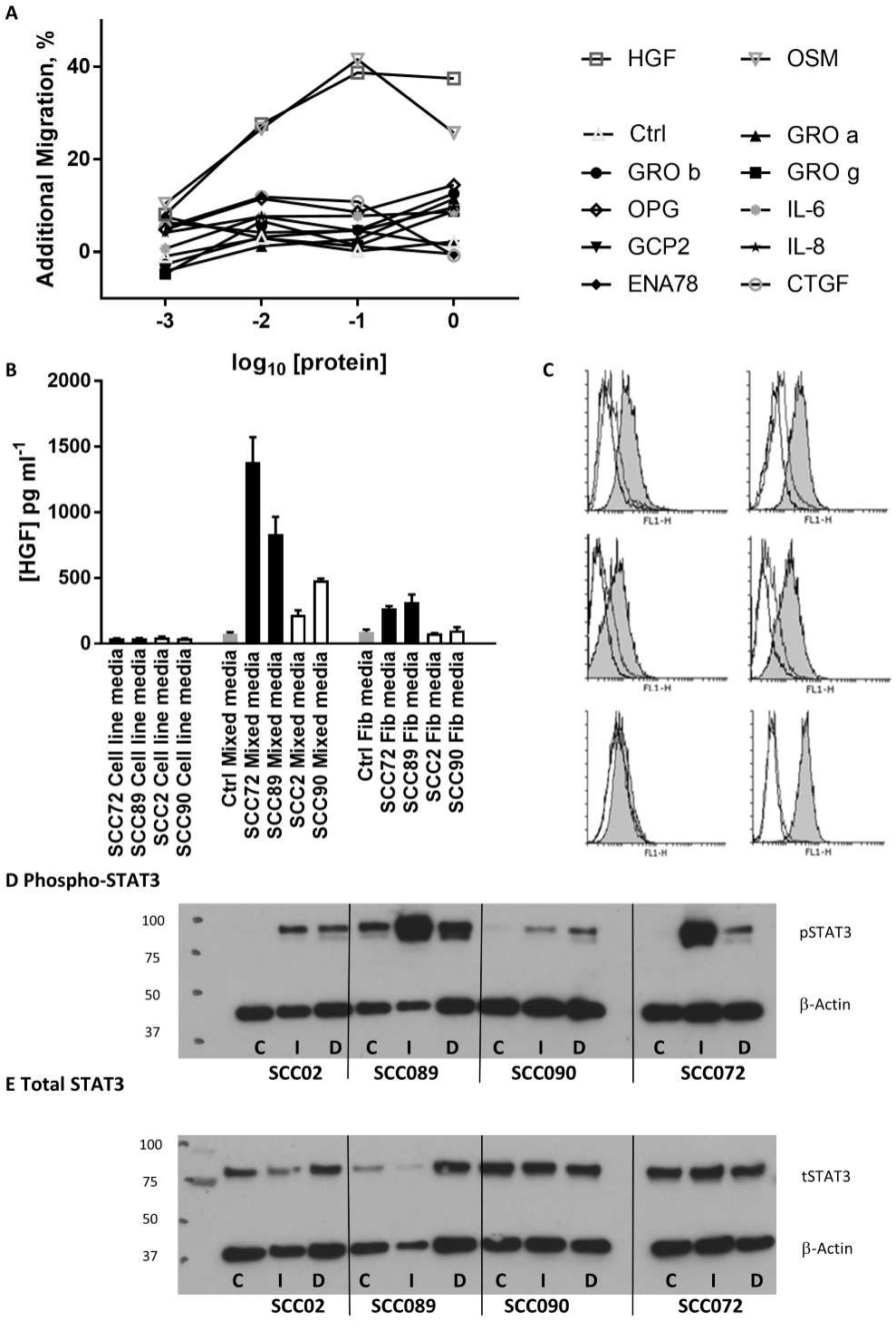
A
Additional Migration, %
40
20
0
-3
-2
-1
0
log10 [protein]
HGF
OSM
Ctrl
GRO a
GRO b
GRO g
OPG
IL-6
GCP2
IL-8
ENA78
CTGF
B
[HGF] pg ml-1
2000
1500
1000
500
0
SCC72 Cell line media
SCC89 Cell line media
SCC2 Cell line media
SCC90 Cell line media
Ctrl Mixed media
SCC72 Mixed media
SCC89 Mixed media
SCC2 Mixed media
SCC90 Mixed media
Ctrl Fib media
SCC72 Fib media
SCC89 Fib media
SCC2 Fib media
SCC90 Fib media
C
FL1-H
D Phospho-STAT3
100
75
50
37
pSTAT3
β-Actin
C I D C I D C I D C I D
SCC02
SCC089
SCC090
SCC072
E Total STAT3
100
75
50
37
tSTAT3
β-Actin
C I D C I D C I D C I D
SCC02
SCC089
SCC090
SCC072

Fig. 4.

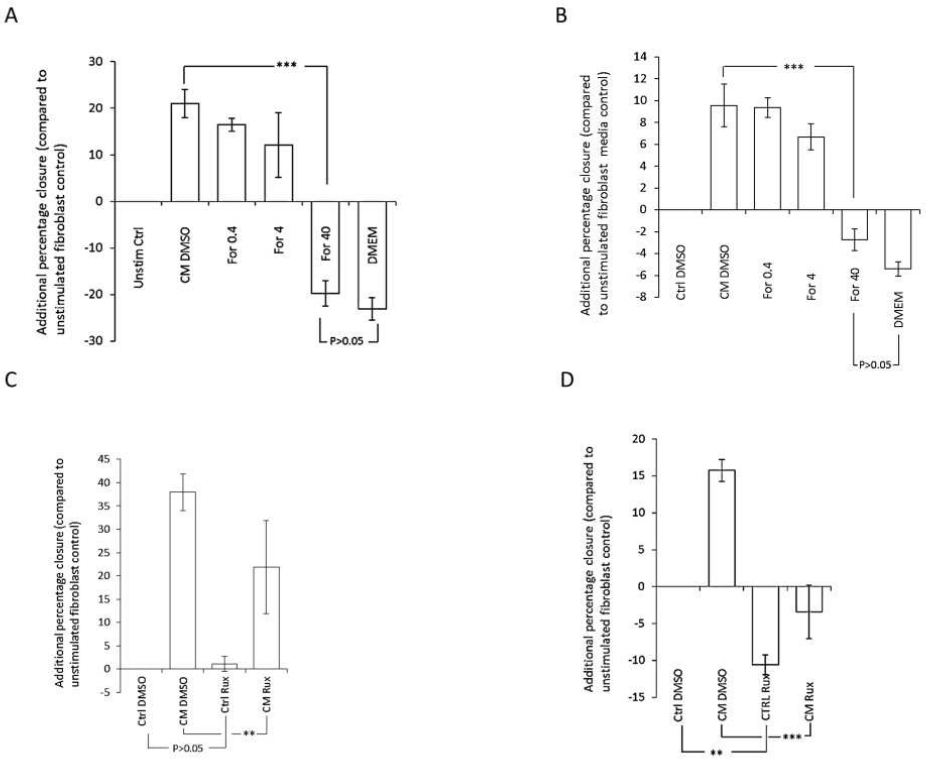
A
Additional percentage closure (compared to unstimulated fibroblast control)
30
20
10
0
-10
-20
-30
***
Unstim Ctrl
CM DMSO
For 0.4
For 4
For 40
DMEM
P>0.05
B
Additional percentage closure (compared to unstimulated fibroblast media control)
14
12
10
8
6
4
2
0
-2
-4
-6
-8
***
Ctrl DMSO
CM DMSO
For 0.4
For 4
For 40
DMEM
P>0.05
C
Additional percentage closure (compared to unstimulated fibroblast control)
45
40
35
30
25
20
15
10
5
0
-5
Ctrl DMSO
CM DMSO
Ctrl Rux
CM Rux
P>0.05
**
D
Additional percentage closure (compared to unstimulated fibroblast control)
20
15
10
5
0
-5
-10
-15
Ctrl DMSO
CM DMSO
CTRL Rux
CM Rux
**
***

Fig. 5.

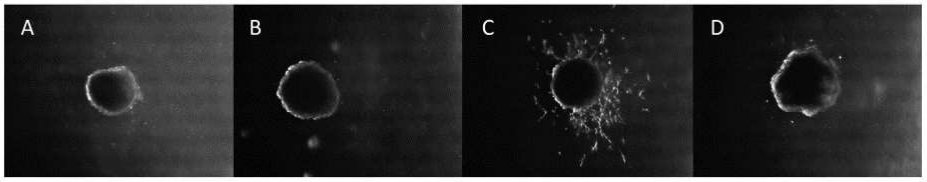
A
B
C
D

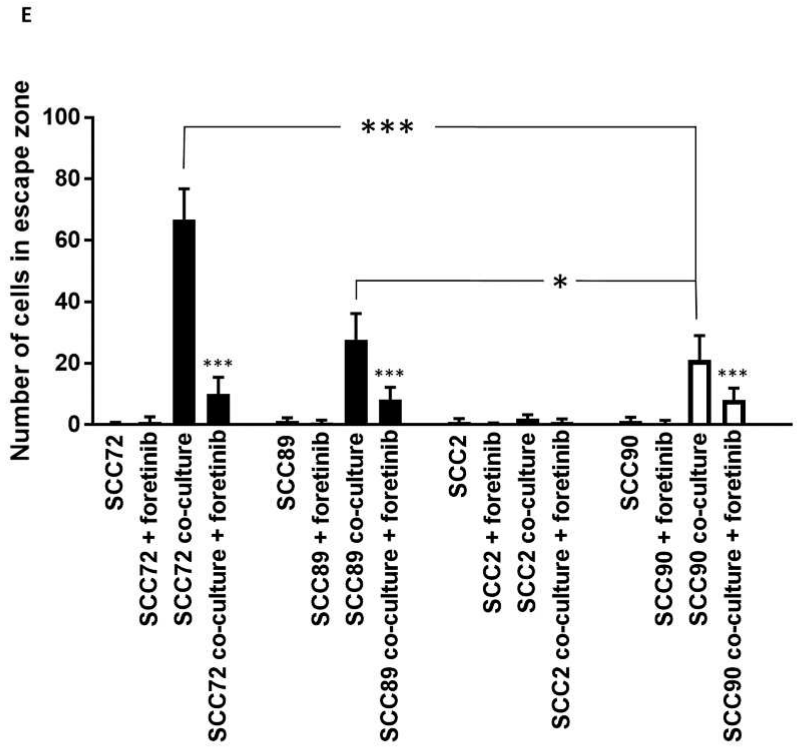
E
Number of cells in escape zone
100
80
60
40
20
0
***
*
***
***
***
SCC72
SCC72 + foretinib
SCC72 co-culture
SCC72 co-culture + foretinib
SCC89
SCC89 + foretinib
SCC89 co-culture
SCC89 co-culture + foretinib
SCC2
SCC2 + foretinib
SCC2 co-culture
SCC2 co-culture + foretinib
SCC90
SCC90 + foretinib
SCC90 co-culture
SCC90 co-culture + foretinib

Fig. 6.

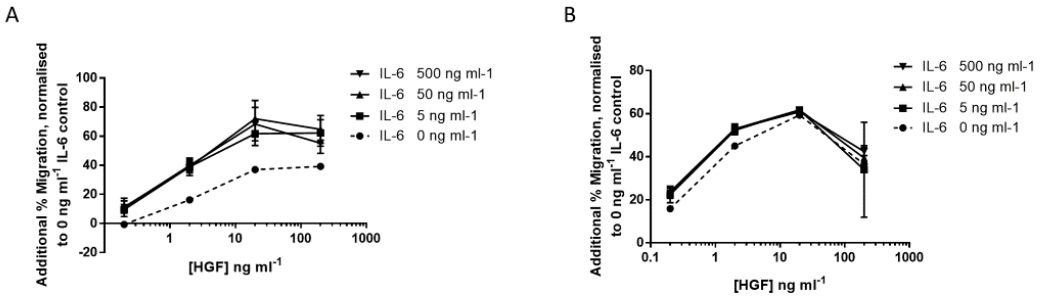
A
Additional % Migration, normalised to 0 ng ml-1 IL-6 control
100
80
60
40
20
0
-20
1
10
100
1000
[HGF] ng ml-1
IL-6 500 ng ml-1
IL-6 50 ng ml-1
IL-6 5 ng ml-1
IL-6 0 ng ml-1
B
Additional % Migration, normalised to 0 ng ml-1 IL-6 control
80
60
40
20
0
0.1
1
10
100
1000
[HGF] ng ml-1
IL-6 500 ng ml-1
IL-6 50 ng ml-1
IL-6 5 ng ml-1
IL-6 0 ng ml-1

Supplemental Figures